Nightside thermospheric FUV emissions due to energetic neutral atom precipitation during magnetic superstorms

Y. Zhang,[1] L. J. Paxton,[1] J. U. Kozyra,[2] H. Kil,[1] and P. C. Brandt[1]

Received 25 March 2005; revised 2 June 2006; accepted 8 June 2006; published 16 September 2006.

[1] TIMED/GUVI detected anomalous FUV emissions from the nightside thermosphere over a wide latitude range, from the subauroral latitudes to the equatorial regions during each of three magnetic superstorms (29–31 October 2003, 20 November 2003, and 7–10 November 2004). We note that during the one case (7–10 November 2004) where there were coincident measurements of the flux of energetic particles as observed by IMAGE HENA, the FUV intensity (as seen in five bandpasses or ''colors'': 121.6 nm, 130.4 nm, 135.6 nm, LBHS (140–150 nm) and LBHL (165–180 nm)) showed qualitative agreement with the behavior of the energetic neutral atoms (ENA). This suggests that the source of the FUV emissions is the ENA originating from the ring current. We also found that for all three storms we studied that the FUV intensities are well correlated with *Dst*. The intensity in all colors is observed to increase with latitude up to the auroral oval. Except for 121.6 nm, the observed intensities exhibit a sharp decrease near the magnetic equator region. The origin, location, and spatial extent of the FUV emissions is quite different from that of the traditional aurora, we find that this phenomena is consistent with neutral particle precipitation. We call this signature of the coupling of the ring current and the thermosphere the neutral particle aurora.

Citation: Zhang, Y., L. J. Paxton, J. U. Kozyra, H. Kil, and P. C. Brandt (2006), Nightside thermospheric FUV emissions due to energetic neutral atom precipitation during magnetic superstorms, *J. Geophys. Res.*, *111*, A09307, doi:10.1029/2005JA011152.

1. Introduction

[2] Space-based observations of emissions in EUV, FUV and visible wavelengths from the nightside thermosphere due to energetic ions and neutral particle precipitation have been reported for decades. Based on observations by STP 72-1 satellite, *Meier and Weller* [1975] found that EUV (17.0–40.0 nm) emission exists regularly at nightside over the magnetic dip equator. The radiation is believed to be λ = 30.4 nm recombination emission from energetic helium ions and appears as a single arc, quite distinct in spatial form from the oxygen emission arcs at 130.4 and 135.6 nm. The magnitude of the EUV emission was reported to be correlated with indices of magnetic activity, indicating that alpha particles scattered downward from the ring current repeatedly recombine and lose electrons as they enter the atmosphere and lose energy. EUV emissions in the wavelength range between 5.0 and 78.0 nm have been detected by a telescope on the Apollo Soyuz in the equatorial region during magnetically quiet time [*Paresce*, 1979]. The observed signals were also interpreted as recombination radiation of energetic helium, and possibly oxygen ions, originating in the terrestrial ring current. However, no enhancement in the 135.6–155.0 nm intensity was noted. During magnetically disturbed periods, data from a spectrometer on the STP 78-1 satellite indicated excess O-I 130.4 nm and 135.6 nm emission within 5° of the dip equator [*Abreu et al.*, 1986]. Neutral particle precipitation from the ring current was discussed as a possible source of the excess emission. Enhanced FUV emissions (e.g., 130.4 nm, 135.6 nm) on both dayside and nightside during magnetic storms are likely the result of precipitating energetic neutral atoms from the ring current [*Stephan et al.*, 2001]. Satellite observations of Doppler shifted Lyman alpha provide direct evidence that precipitating H/H+ are the source of proton aurora [*Ishimoto et al.*, 1989]. *Stephan et al.* [2004] found that enhanced oxygen ion and neutral line above 300 km in the dusk side auroral oval during a storm recovery could be due to precipitating O^+ from the ring current. The enhancement in the FUV limb intensities at midlatitude and small ratio between 1304.nm and 135.6 nm intensities during magnetic storms indicate that ENA are the source of the enhanced FUV emissions [*DeMajistre et al.*, 2005].

[3] In addition to the satellite measurements, ground-based observations also support the idea that the particles from the ring current cause enhanced emission in the low-latitude and equatorial regions. *Tinsley* [1979] reported observations of hydrogen Balmer β and He^+ 468.6 nm emissions at Huancayo, Peru during two storms. Such emissions are consistent with energetic neutral atom precipitation resulting from charge-exchange loss of ring current ions. On the basis of observation of H Balmer β emission during an intense magnetic storm (29 September 1978 with

[1]Johns Hopkins University Applied Physics Laboratory, Laurel, Maryland, USA.
[2]Space Physics Research Laboratory, University of Michigan, Ann Arbor, Michigan, USA.

0148-0227/06/2005JA011152

minimum Dst around −224 nT), *Tinsley and Burnside* [1981] demonstrated that energetic hydrogen atoms or protons were involved. Of these, H atoms are the more plausible explanation [*Tinsley and Burnside*, 1981]. They also reported that the N_2^+ 427.8 nm intensity increases with decreasing Dst. Observations of H Balmer β and other emissions at different low and midlatitude sites (Mt. Haleakala, Hawaii and Cachoeira Paulista, Brazil, McDonald Observatory, southwest Texas) also indicate the precipitation of energetic neutral atoms and/or ions originating in the ring current [*Rohrbaugh et al.*, 1983]. Ground-based observations of anomalously high N_2^+ First Negative vibrational/rotational temperature (∼4000°k) at low latitudes also provide evidence of precipitation of energetic ions or neutral atoms [*Rassoul et al.*, 1993, and references therein].

[4] All these earlier observations were based on either photometers or spectrometers. Their spatial coverage was rather limited. Furthermore, the conclusion that the source is energetic neutral particle precipitation is based on theoretical arguments as there were no coincident ENA measurements made during the earlier observations. Here we report TIMED/GUVI imaging observations of FUV emissions due to the energetic neutral particle precipitation during three superstorms and simultaneous IMAGE measurements of energetic neutral atoms (ENAs) during one superstorm.

[5] Energetic neutral atom (ENA) imaging was first conceptualized by *Roelof et al.* [1985] and has become an important tool for space plasma diagnostics. ENA images of the ring current have been obtained from several spacecraft [*Roelof*, 1987]. Dedicated ENA imagers have been carried by the Astrid satellite [*Barabash*, 1995], Cassini [*Mitchell et al.*, 1998], and now IMAGE [*Mitchell et al.*, 2000].

[6] There are many names used to describe the emissions due to neutral particle precipitation, such as equatorial aurora [*Paresce*, 1979; *Tinsley*, 1979], tropical ultraviolet nightglow [*Knudsen*, 1970], and midlatitude aurora [*Torr and Torr*, 1984] and heavy particle aurora [*Rassoul et al.*, 1993]. Because GUVI observations have better coverage in space and time and are able to better characterize the morphology, behavior, and origin of these phenomena, we find that these emission appear to be solely due to the precipitation of neutral particles. Thus we propose calling the emissions neutral particle aurora (NPA) as being more indicative of their nature.

[7] It should be noted that NPA are different from the equatorial arcs in the view of both mechanism and morphology. Note that there is a component of the 130.4 and 135.6 nm emission that arises from the recombination of O^+ ions and thermal electrons in the *F* region ionosphere. The equatorial arcs are produced by radiant recombination of ionospheric O^+ and electrons and they are confined to the equatorial and mid/low latitude regions. Furthermore, the equatorial arcs are observable almost all the time. The GUVI observations of the enhancement of the 121.6 nm signal indicate the presence of precipitating hydrogen atoms during the event. The NPA emissions in LBHS and LBHL are mainly due to the impact of secondary electrons on atmospheric N_2. The NPA 135.6 nm and 130.4 nm emissions are caused by both precipitating ENA O and collisions between the atmospheric O/O_2 and the secondary electrons. We report GUVI observations of the NPA and note that the NPA extend from the equator to the auroral oval in both hemispheres and is only detectable during magnetic storms.

2. Data

[8] Global Ultraviolet Imager (GUVI) is one of four scientific instruments aboard the NASA Thermosphere Ionosphere Mesosphere Energetics and Dynamics (TIMED) satellite. TIMED was launched on 7 December 2001 into a 630 km circular polar orbit with an inclination of 74°. GUVI provides cross-track scanned images of the Earth's ultraviolet airglow and auroral emissions in the far ultraviolet (FUV) at wavelengths 115.0 to 180.0 nm. Major emission features include HI (Lyman α, 121.6 nm), OI (130.4 nm), OI (135.6 nm) lines, N_2 LBHS band (140.0–150.0 nm), and N_2 LBHL band (165.0–180.0 nm). Images are generated using a microprocessor-controlled cross-track scan mirror mechanism that scans the disk beginning 60° from nadir on the sunward side across the disk and through the limb on the antisunward side of the satellite [*Paxton et al.*, 1999; *Paxton and Meng*, 1999; *Christensen et al.*, 2003; *Paxton et al.*, 2004].

[9] The Imager for Magnetopause-to-Aurora Global Exploration (IMAGE) satellite carries a High Energy Neutral Analyzer (HENA) that detects energetic neutral atoms in the 10 to 500 keV energy range [*Mitchell et al.*, 2001]. Energetic neutral atoms are produced when singly and positively charged ions undergo change exchange collisions with cold neutral atoms or molecules. The ions will become neutral and travel on trajectories that are unaffected by electromagnetic fields. In the terrestrial magnetosphere, the ring current ions will charge exchange with the geocorona at high altitudes and emit ENAs. Part of the ENAs will escape into the magnetosphere. Since the initial energy is much greater than the planetary escape energy (0.6 eV/nucleon), the ENA are not affected by gravitation fields and effectively travel in straight lines. In this way, the ring current ions can be imaged by the HENA sensor that records the arrival direction and velocity of the energetic neutral atoms (52–180 keV O, 10–60 keV H, and 60–198 keV H) created by the ring current-exosphere interaction [*Roelof and Skinner*, 2000]. HENA is a slit camera with a 90° × 120° field of view [*Mitchell et al.*, 2000]. This large field of view enables HENA to detect global ring current distribution most of time despite changes in the IMAGE position (apogee: 46,000 km, perigee: 1000 km). Because the exosphere is relatively stable in distribution and density, images of ENA can be inverted to retrieve the original global ring current ion distribution [*Roelof and Skinner*, 2000; *Brandt et al.*, 2002]. Part of the ENA will precipitate into the atmosphere and cause FUV emissions that can be detected by GUVI.

3. Events

[10] In this paper we report the first two-dimensional (2-D) FUV imaging observation of neutral particle aurora. NPA are quite different from the traditional aurora in the auroral oval and detached aurora at subauroral latitudes.

3.1. Case on 20 November 2003

[11] Superstorms are defined as the magnetic storms associated with a Dst less than −240 nT [*MacMahon and*

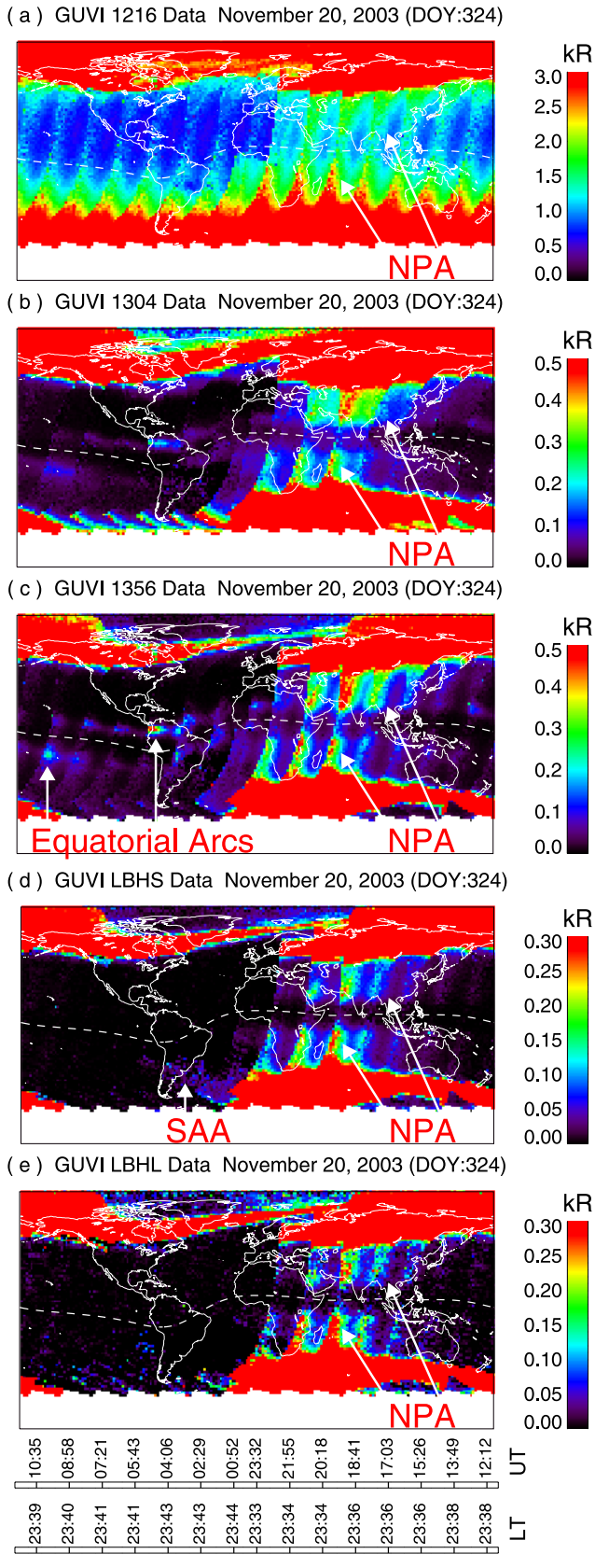

Figure 1. GUVI intensity maps of the nightside radiance on November 20, 2003: (a) 121.6 nm, (b) 130.4 nm, (c) 135.6 nm, (d) LBHS, and (e) LBHL. Note UT starts in the middle of the plots and goes in a right-to-left direction due to Earth rotation and TIMED orbits at a nearly fixed local time.

Gonzalez, 1997]. A superstorm occurred on 20 November 2003 with Dst reaching as low as −472 nT. During this storm, nightside detached aurora (NDA) at subauroral latitudes due to direct precipitation of the ring current protons/ions were detected [*Zhang et al.*, 2005]. The NDA are limited to a narrow range of magnetic latitudes (45°−55°) and MLT (1900 to 2400 and 0300) and should not be confused with the observation of a much broader region of NPA.

[12] Figure 1 shows plots of GUVI disk scanning images in five "colors" (121.6 nm, 130.4 nm, 135.6 nm, LBHS and LBHL) on the nightside during 20 November 2003. The plots are generated from GUVI data over a whole day (15 orbits). GUVI image data for each orbit cover a roughly south-north orientated swath with a width of ∼2500 km. The UT and local time (LT) at the bottom of Figure 1 are marked for GUVI nadir pixels near the equator. The LT ranges from 2333 to 2343, indicating the GUVI images are obtained near midnight. Note the UT starts in the middle of the plots and increases toward the left. The GUVI images in the left half of the plots (between 0000 and 1035 UT) indicate a magnetically quiet nightside FUV emission in middle, low, and equatorial latitudes: relatively smooth 121.6 nm intensity, some enhancement in 130.4 nm and 135.6 nm intensities on both sides of the magnetic equator (indicated by the white dashed line) due to equatorial arcs, and no detectable emission in LBHS and LBHL. The apparent LBH signal in the South Atlantic Anomaly (SAA) region is caused by spurious events in the GUVI detector and is not actually indicative of atmospheric emissions. Around 1212 UT, an intensity enhancement was seen in the 121.6 nm data (Figure 1a). The enhancement is rather uniform and covers all latitudes from the equatorward edge of the northern auroral oval to the edge of the southern auroral oval. However, there is strong look-angle (in the longitude direction) dependence. This look angle dependence means that GUVI was measuring real emissions from the atmosphere as this look angle dependence is characteristic of the changing viewing geometry. The emissions also show a clear altitude dependence in the limb profiles with a peak altitude of about 140−180 km. If we look carefully, enhancements in other four GUVI "colors" (Figures 1b to 1e) are also first seen around 1212 UT. However, the enhancements are more easily identified around 1703 UT. Figures 1b−1e basically shows the same feature as seen in Figure 1a, except that the intensity diminishes around the magnetic equator. The relatively uniform latitude dependence suggests that the emissions are due to neutral particles, a source mechanism unaffected by the Earth's magnetic field. For this reason, we call these observed emissions neutral particle aurora. Section 3.3 will present evidence of the correlation between the GUVI and IMAGE HENA observations.

[13] In order to see the correlation between the NPA intensity and the ring current (Dst), we plot, in Figure 2, the GUVI nightside mean intensities (circles) of each scan between −16° and 16° geographic latitudes with Dst over 2 days (20−21 November 2003). Figures 2a−2d (GUVI 121.6 nm, 135.6 nm, LBHL, LBHS) show that the GUVI intensities are enhanced during the later half day on 20 November 2004 (DOY 324). Note that the 135.6 nm emissions show two separated enhancements due to the radiative recombination in the equatorial arcs. These

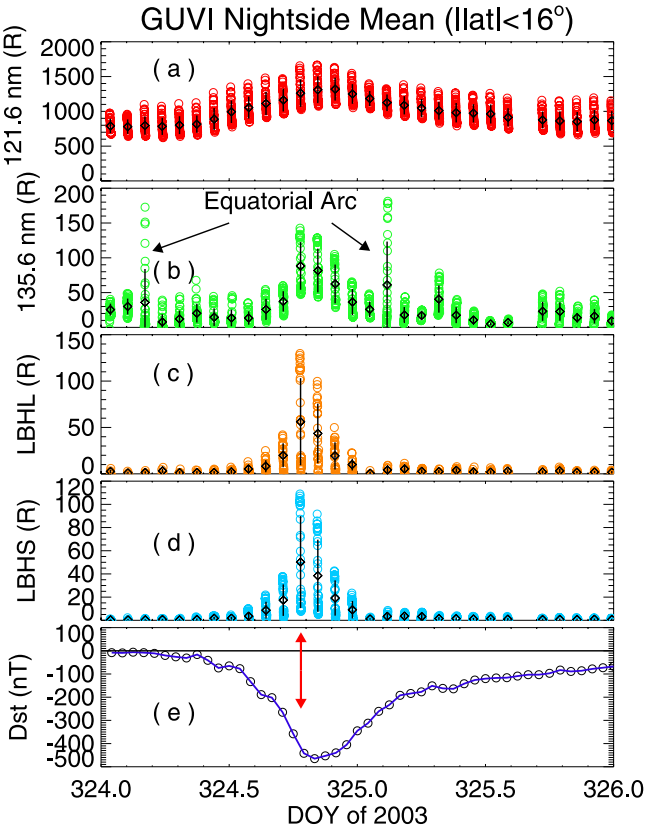

Figure 2. (a)–(d): GUVI mean intensities of each scan in the nightside equatorial region (−16° < latitude < 16°) and (e): Dst plot over a two-day period (November 20–21, 2003, DOY: 324–325). The black diamonds and vertical lines are for the average and statistical error levels of each group, respectively.

enhancements are marked in Figure 2b. Because the position of the equatorial arcs follows the magnetic equator and the geographic latitude of the magnetic equator changes with the geographic longitude (see Figure 1), some of the equatorial arcs are not visible in Figure 2b. GUVI 130.4 nm data are not shown because they are similar to the 135.6 nm data. Note the circles in Figures 2a–2d are grouped for each orbit. The black diamonds and vertical lines are for the average and statistical error levels of each group, respectively. The red arrow in Figure 2e (Dst plot) marked the time when GUVI detected the most intense NPA. This is associated with a low Dst and large rate of decrease in Dst. Once Dst started to decrease around 1000 UT on 20 November 2003 (2 hours before DOY = 324.5), all the FUV intensities began to increase, especially the 121.6 nm intensity. After the Dst reached its minimum of −472 nT, the NPA intensities started to decrease. Over all, the NPA intensities are well correlated with Dst. One interesting feature is that the LBHS and LBHL intensities in the NPA are about the same. This feature exists for the other cases as discussed in sections 3.2 and 3.3.

3.2. Cases on 29–31 October 2003

[14] Three NPA events were observed during a 3-day period from 29 to 31 October 2003. Figure 3, similar to Figure 1d, shows the enhanced nightside GUVI LBHS intensities due to the NPA. The three NPA events occurred during three major magnetic storms observed between 29 and 31 October 2003 (DOY 302–304) (see Figure 4e). They are marked by three red arrows. The lowest Dst associated with them are −180, −363, and −401 nT, respectively. The last two storms are identified as superstorms. Each of the storms causes an enhancement in the GUVI intensities in the nightside between −16° and 16° latitudes (see Figures 4a–4d). The first storm (the weak one) leads to a small increase in the GUVI intensities, whereas the last two intense storms cause a big enhancement in the GUVI intensities. These three storms in sequence further support hypothesis that there is a correlation between NPA intensities and Dst. In addition to the three peaks in the 121.6 nm intensity (Figure 4a), the 121.6 nm intensity also shows a decreasing trend over the 3 days. This is due to the precession of GUVI orbit from 0404 LT on 29 October to 0330 LT on 31 October and decrease in solar EUV flux (the F107 fluxes are 275.4, 267.6, and 245.2 for the 3 days, respectively). Again, Figure 4 shows a good correlation between the GUVI NPA intensities and Dst.

3.3. Cases on 7–10 November 2004

[15] Three intense magnetic storms were observed between 7 and 10 November 2004. Three NPA events were detected by GUVI during 8–10 November 2004 (see Figure 5). The magnetic storms are marked using three red arrows in Figure 6f. The corresponding lowest Dst are −383, −231, and −296 nT, respectively. The first and third storms are superstorms. Just like the cases presented in sections 3.1 and 3.2, the first storm in late 7 November and early 8 November 2004 leads to significant enhancement in GUVI 121.6 nm, 130.4 nm, 135.6 nm, LBHL and LBHS intensities (Figures 6a–6d, 130.4 nm data not shown). IMAGE HENA data are also available during most of the 4-day period. Total fluxes of HENA (52–180 keV O, 10–60 keV H, and 60–198 keV H) are plotted in Figure 6e. The data gaps in the IMAGE data in Figure 6e are due to either the lack of data or the data were contaminated by MeV particles. Nevertheless, HENA fluxes are correlated with the GUVI intensity enhancement during the first storm. The growth phase of the second storm lasted a very short time (~2 hours), consequently GUVI detected NPA over one orbit (see Figures 6b–6d). NPA in the third storm can be clearly seen in Figures 6b–6d. However, enhancements in the 121.6 nm intensities due to the last two storms are rather small, though they can still be identified in Figure 6a. We note that the 121.6 nm geocoronal intensities do not change very much during the period. This is to be expected as the LST of the observations is nearly constant (from 0151 to 0121 over the 4 days) and the solar flux as measured by the TIMED SEE solar irradiance (30.0–31.0 nm) daily average varied from 0.36 to 0.38 mW/m^2/nm over the 4-day period.

[16] We examined the correlation between coincident GUVI mean intensities (see Figures 6a–6d) and HENA total fluxes (Figure 7). The geocoronal component in the GUVI 121.6 nm data has been removed in Figure 7a. Considering that the time resolution of IMAGE HENA data is 2 min and it takes about 10 min for GUVI to scan through the equatorial region from −16° to16° latitude, a 10-min difference is allowed when determining the GUVI and HENA coincidence in time. Despite relatively large scatter, Figures 7a–7b shows a quasi-linear correlation between

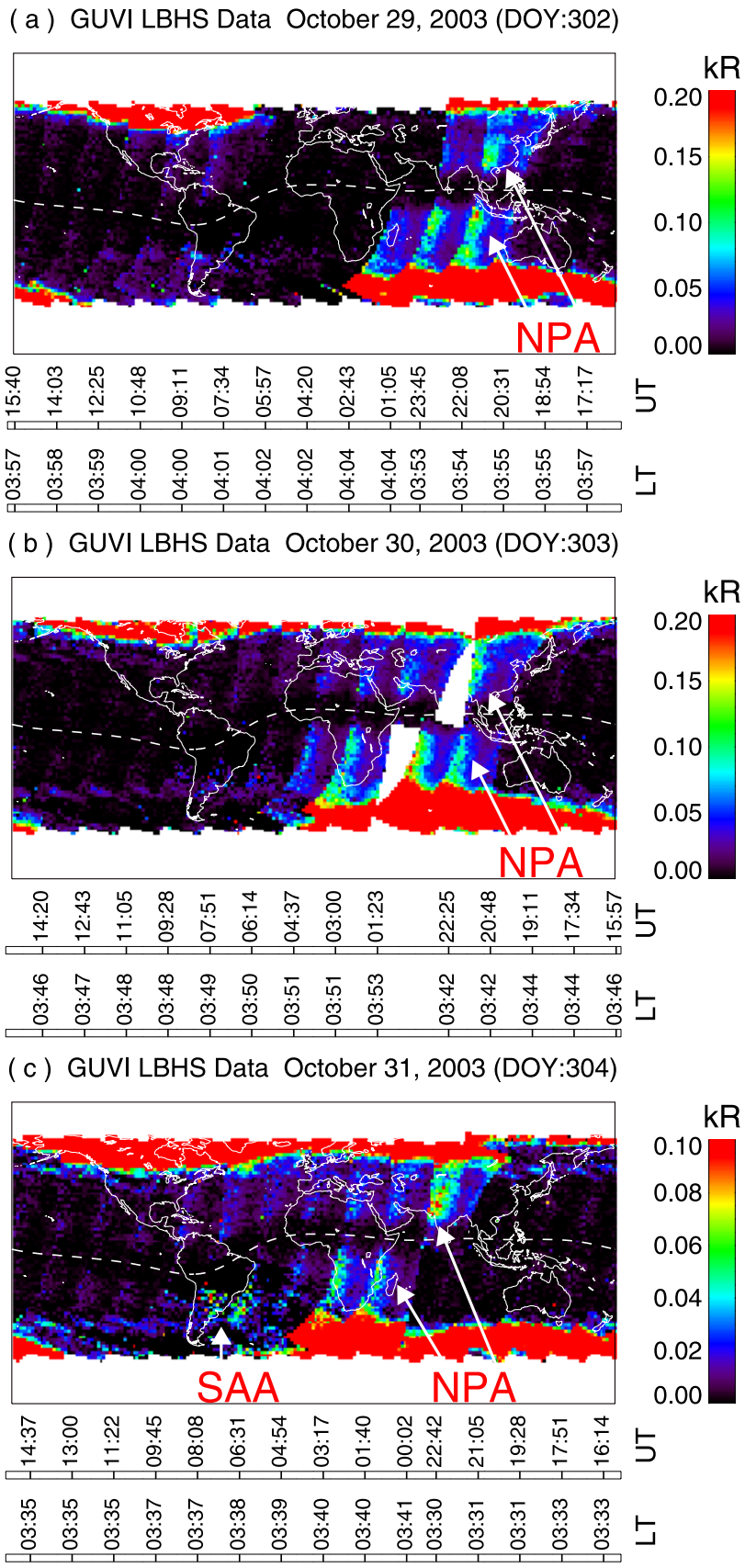

Figure 3. GUVI LBHS nightside images on (a) October 29, (b) October 30, and (c) October 31, 2003. NPA were observed on each of the three days.

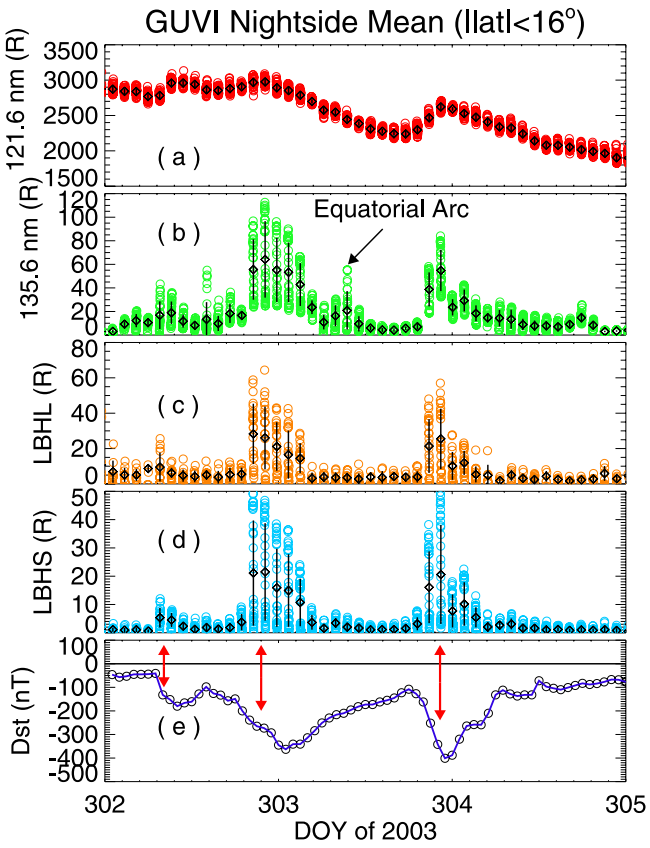

Figure 4. Similar to Figure 2, but for October 29–31, 2003 (DOY: 302–304).

GUVI 121.6 nm intensities and HENA total fluxes of 10–60 keV H and 60–198 keV H (the linear correlation coefficients are 0.749 and 0.529, respectively). A fairly good linear correlation exists between other GUVI (130.4 nm, 135.6 nm, LBHS, LBHL) intensities and HENA 52–189 keV O flux (Figures 7c–7f, the linear correlation coefficients are 0.916, 0.894, 0.924, and 0.888, respectively). On the other hand, it does not show a good linear correlation (not shown here) between the GUVI intensities other than 121.6 nm and the HENA H fluxes. This suggests that the GUVI 130.4 nm, 135.6 nm, LBHS and LBHL emissions may be mainly excited by energetic O precipitation, while the GUVI 121.6 nm emissions are due to energetic hydrogen atom precipitation.

[17] The NPA intensities are directly controlled by the flux of energetic neutral atoms from the ring current. However, measurements of ENA are not always available and do not cover the entire energy range of the ENA that create NPA. Sometimes the data from IMAGE HENA are contaminated by MeV particles (for the cases on 29–31 October 2003 and 20 November 2004). It is worth comparing the intensities of the NPA with Dst index. Figure 8 shows a scatterplot between GUVI NPA mean intensities and Dst, where the geocorona contribution has been removed in the GUVI 121.6 nm data. Figure 8 is obtained using all the data shown in Figures 2–4. There is a clear negative correlation between the GUVI intensities and Dst, though the correlation is either linear or nonlinear, depending on the Dst values. The GUVI 121.6 nm intensities tend to saturate for a strongly negative Dst (<−200 ~ −300 nT, see Figure 8b). The GUVI 130.4 and 135.6 nm intensities show a quasi-linear or weak nonlinear relationship with Dst, regardless the Dst values. One the other hand, GUVI LBHS and LBHL intensities appear to increase exponentially when the Dst is below −200 nT.

4. Discussion

[18] GUVI observations have revealed several new features of neutral particle aurora during superstorms. Some of the features can be readily explained. Others will need modeling and additional analysis and will be the subject of future papers.

[19] The NPA emissions in the magnetic equator region are significantly weaker than those at midlatitudes in four (130.4 nm, 135.6 nm, LBHS, and LBHL) GUVI "colors" in all the cases (e.g., Figure 1 for case on 20 November 2003). However, the percentage decrease in the 121.6 nm data is much smaller. The emissions in the four GUVI "colors" are due to interaction between the neutral atmosphere species (such as O, N_2, O_2) and the secondary electrons created by impact of energetic neutral particles and precipitating ENA O for the 130.4 and 135.6 nm emissions. Their intensity depends on the incident ENA flux and energy as ENA produces secondary electrons. The weak NPA emission around the magnetic equator must be due to fewer ENA precipitated into the lower atmosphere in that region. Model calculations confirm that the rate of ENA flux [*Tinsley*, 1979], energy deposition by ENA [*Noel and Proelss*, 1993], and ionization production by ENA [*Bauske et al.*, 1997] have their minimum values around the magnetic equator during early stage of a magnetic storm.

[20] We know that the 121.6 nm emission is directly from the H/H+ precipitation (i.e., secondary electrons are an ineffective source) and emissions in other four GUVI colors are from the secondary electron (created by all energetic particle precipitation) impact on neutral atmosphere and/or directly from precipitating O/O^+ precipitation. The different behavior of 121.6 nm intensity at the magnetic equator indicates that emissions in the other four colors are less correlated with the ENA H precipitation and they are probably mainly due to ENA O precipitation. It also suggests that the total energy flux of ENA O may be significantly larger than that of ENA H. For a better understanding of the phenomenon, computer simulations are needed.

[21] We believe that energetic H precipitating from the ring current is the source for the enhanced 121.6 nm emission observed during these superstorms. This provides an opportunity to model the relation between the enhanced 121.6 nm and energetic H flux. Figures 7a–7b shows that the maximum 121.6 nm intensity of NPA is around 500 R. To estimate the 121.6 nm intensity for a given H^+/H energy and flux or vice versa, we did a number of B3C [*Daniell*, 1993] runs for monoenergy H/H^+ beams with their energy varying from 1 to 200 keV (see the diamonds in Figure 9). The B3C runs (Figure 9) show that the simulated 121.6 nm intensity (solid line, viewed from a satellite) decreases rapidly and nonlinearly with the characteristic energy of H^+/H that precipitate in a nadir direction. Note the calculations were done for a fixed energy flux of 1 ergs/s/cm^2. The dashed line in Figure 9 is the simulated total H^+/H number flux required to produce 500 R of 121.6 nm emission. The H^+/H with

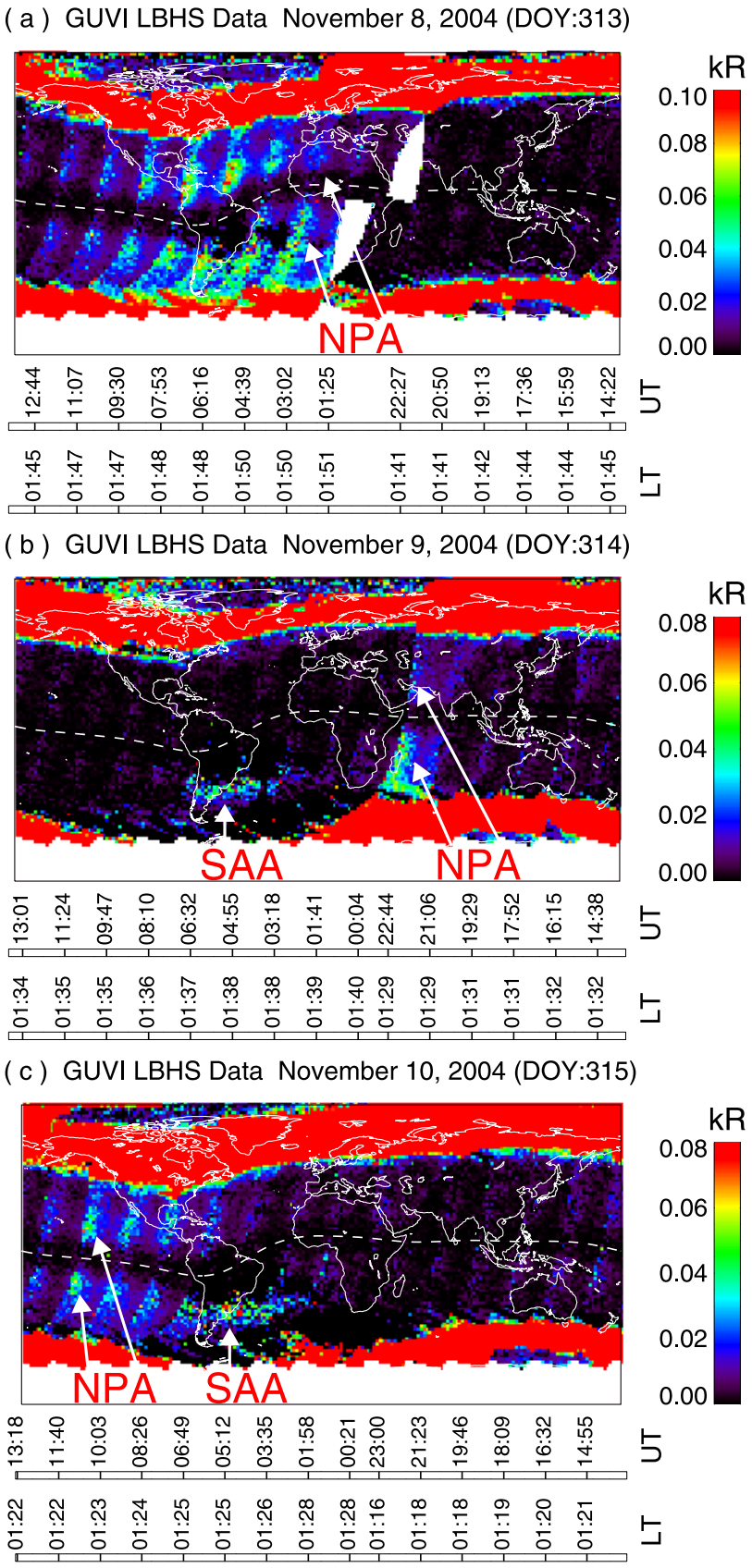

Figure 5. GUVI LBHS nightside images on (a) November 8, (b) November 9, and (c) November 10, 2004. NPA were observed on each of the three days.

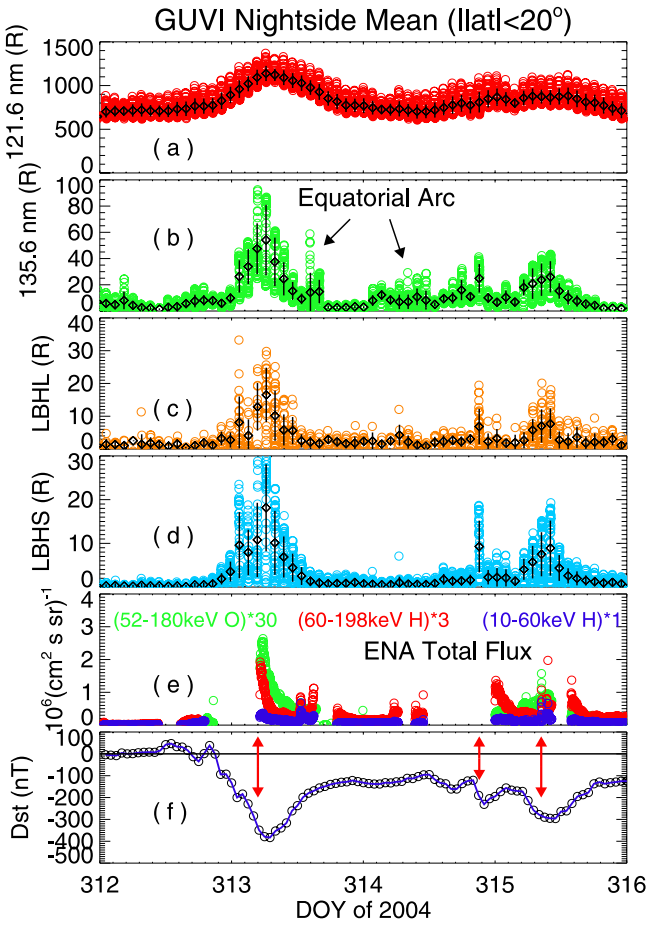

Figure 6. (a)–(d): GUVI mean intensities of each scan in the nightside equatorial region (−20° < latitude < 20°), (e) IMAGE HENA total flux for 52–180 keV O (green), 60–198 keV H (red), 10–60 keV H (blue) and (f): Dst plot over a four-day period (November 7–10, 2004, DOY: 312–315).

energy around 25 keV are the most efficient in creating the 121.6 nm emission and need a minimum number flux of 8.0×10^5 cm^{-2} s^{-1}. The simple B3C runs provide an indication that future modeling studies are required for a better understanding of the observations.

[22] One of the interesting features of NPA is that the LBHS and LBHL intensities are roughly the same at latitudes up to the auroral oval (see Figures 1d and 1e). Also see the detailed analysis of the ratios for latitudes from −16° to 16° (Figures 2 and 3) and from −20° to 20° (Figure 6). The ratios of the LBHS and LBHL intensities are independent of look angle on the disk. Note that magnetic storms can cause significant depletions in the O density but only a few percent of change in the N_2 and O_2 densities in the thermosphere. Therefore the LBHS and LBHL intensities of the NPA are determined by the total flux and spectral shape of the ENAs. Considering the good correlation between both the NPA LBHS and LBHL intensities and the 52–180 keV O fluxes (Figures 7e–7f), and the fact that the cross sections for momentum transfer on atmospheric constituents are considerably larger for oxygen than for hydrogen [*Torr and Torr*, 1979], we suggest that the energetic O precipitation is the major source of the LBHS and LBHL emission. The limb data have the potential to provide the means to constrain the estimate of the energy spectrum and we plan to investigate this further. GUVI observes the peak in the emission at altitudes of about 155–190 km for OI 135.6 nm and LBHS emissions and 140–175 km for LBHL. We need to do a more detailed modeling study to find the effective energy of ENA H and O based on the peak emission heights.

[23] Figure 8 has demonstrated that GUVI NPA intensities in the low and equatorial regions are correlated with Dst. The 121.6 nm intensities seems to have a smaller degree of change once Dst <−300 nT (see the solid line, a least squares polynomial fit, in Figures 8a and 8b). The GUVI 130.4 nm and 135.6 nm intensities appear to have a quasi-linear or weak nonlinear relation with Dst (see the solid curve in Figures 8b–8c). The GUVI LBHS and LBHL intensities, however, increase exponentially with decreasing Dst (<−200 nT) (see the exponential fit in Figures 8e–8f). These differing NPA intensities may be explained by two factors. (1) During intense storms, the ring current mainly consists of H^+ and O^+ ions. The total ring current population increases with decreasing Dst. Furthermore, the fraction of O^+ population increases with decreasing Dst [*Daglis et al.*, 1999, *Fu et al.*, 2001]. Therefore the total O^+ (and the total ENA O) flux increases nonlinearly with decreasing Dst. Note that based on the morphology of the observed emissions, the ENA O from the ring current O^+ is the dominant source for the LBHS and LBHL. The increase in O^+ leads to the nonlinear increase in the LBHS and LBHL intensities. On the other hand, the storm-time thermospheric O depletion in the nightside thermosphere occurs in the 1–3 hours after a storm starts. Competition between the reduction of atmospheric O density and the increase in the ENA O flux versus Dst may explain the observed quasi-linear relation between 130.4 and 135.6 nm intensities and Dst. (2) The fraction of H^+ population in the ring current decreases with decreasing Dst. Thus the rate of increase of the total H^+ (or the ENA H) flux becomes smaller with decreasing Dst and leads to the saturation effect of the 121.6 nm intensity visible in Figures 8a and 8b.

5. Summary

[24] Superstorms provide the best opportunity for GUVI to detect neutral particle aurora. However, NPA are not limited to the superstorms. Some weaker Dst excursions also lead to detectable NPA as presented in section 3. On the basis of cases presented here, the unique features of NPA can be summarized here.

[25] 1. There is a good correlation between NPA intensities, Dst (all cases), and ENA flux (based on one available case). The 121.6 nm intensities increase with decreasing Dst linearly (−200 nT Dst <0 nT) and tend to saturate when Dst <−300 nT. The 130.4 nm and 135.6 nm intensities increase quasi-linearly with decreasing Dst. The LBHS and LBHL intensities increase linearly (−200 nT < Dst <0 nT) and nonlinearly or exponentially (Dst <−200 nT) with decreasing Dst.

[26] 2. Two factors are important in explaining the GUVI observations: (1) the total ring current ion flux (mainly H^+ and O^+) increases quasi-linearly with decreasing Dst, (2) the

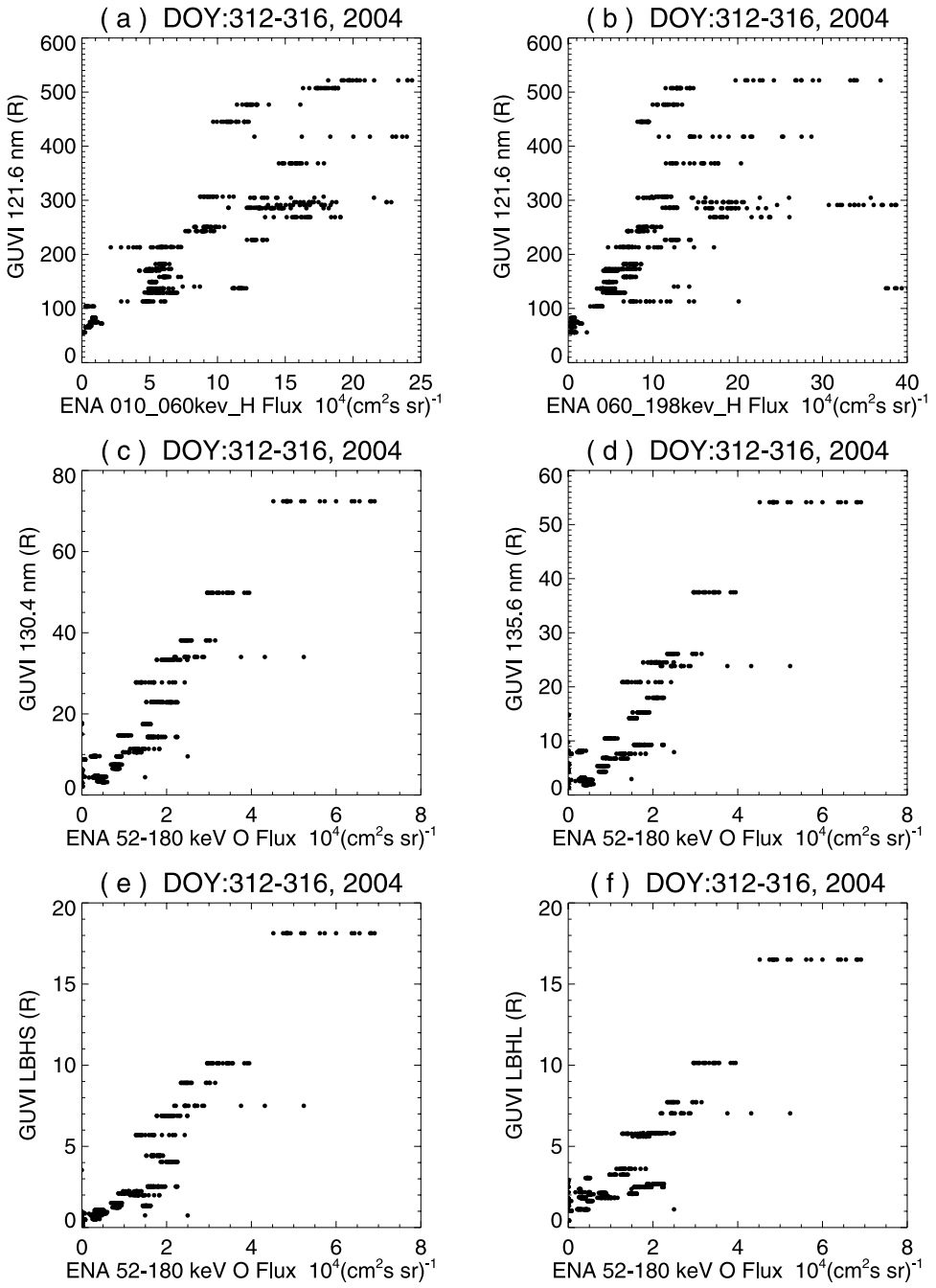

Figure 7. Scatterplots of GUVI mean intensities of each scan versus the coincident IMAGE ENA total fluxes: (a) 121.6 nm (geocorona removed) versus 10–60 keV H, (b) 121.6 nm versus 60–198 keV H, (c) 130.4 nm versus 52–180 keV O, (d) 135.6 nm versus 52–180 keV O, (e) LBHS versus 52–180 keV O, and (f) LBHL versus 52–180 keV O. The linear correlation coefficients for the six plots in Figure 7a–f are 0.749, 0.529, 0.926, 0.894, 0.924, and 0.888, respectively.

fraction of the H^+ decreases and O^+ increases with decreasing Dst. These two factors lead to saturation of total H^+ (and ENA H) flux and a nonlinear increase in the total O^+ (and ENA O) flux at large negative values of Dst. This explains the results in item (1). This also suggests that the emissions in the four GUVI "colors" (excluding the 121.6 nm) are mainly due to ENA O.

[27] 3. Except for the 121.6 nm, NPA intensities in other four "colors" exhibit a sharp decrease in the magnetic equator region between the northern and southern equatorial arcs.

[28] 4. There is a general trend that NPA intensities slowly increase with magnetic latitudes.

[29] Further, more detailed model calculations will be needed to evaluate the interchange of H^+, O^+, O and H that

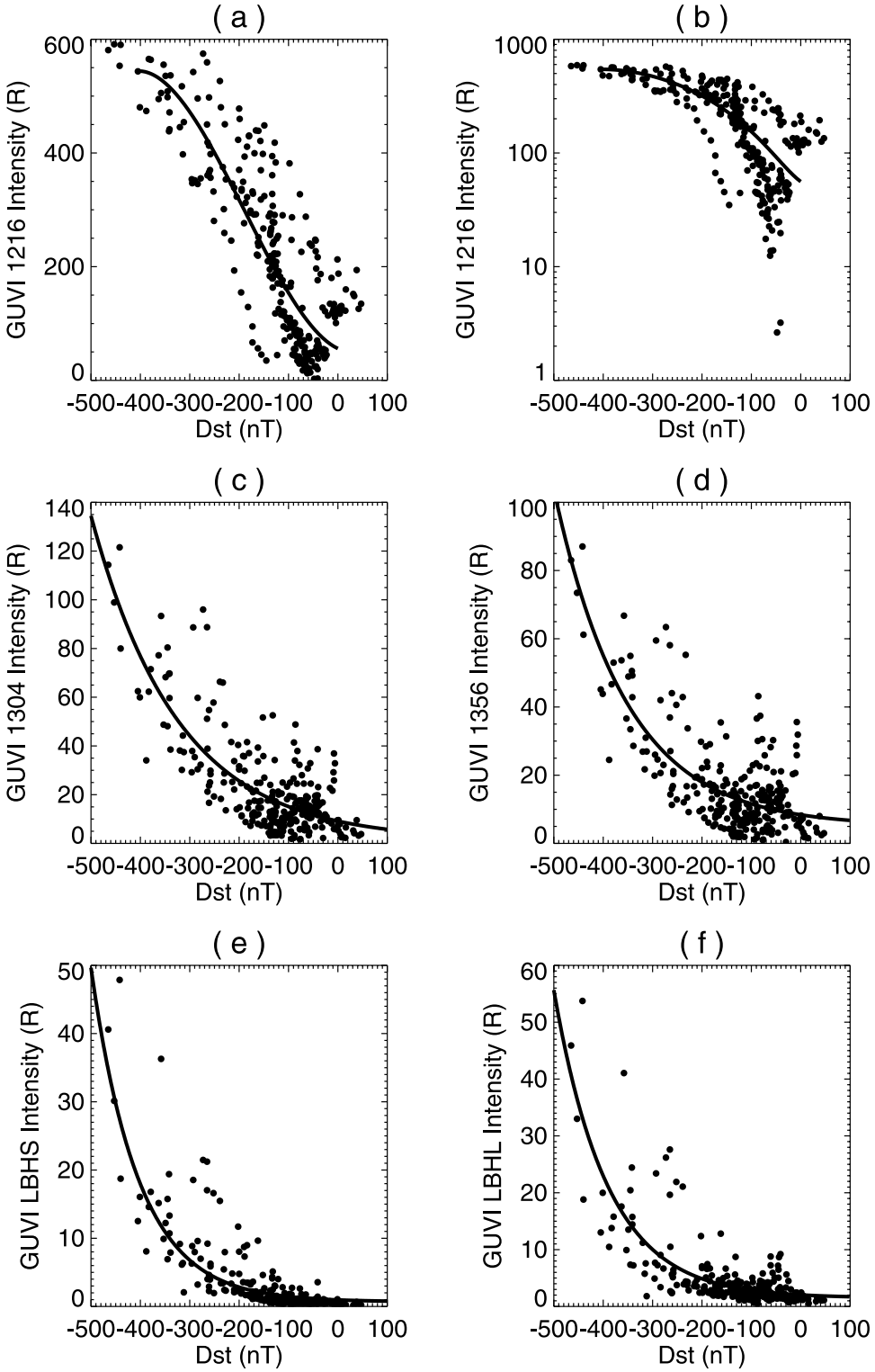

Figure 8. (a)–(f): a scatterplot of GUVI mean intensities (121.6 nm, 130.4 nm, 135.6 nm, LBHS, and LBHL) versus Dst from all the cases presented in Section 3. The geocorona component in the GUVI 121.6 nm intensities has been removed. The solid lines show curves of minimum-square polynomial (Figure 8a,b) and exponential (Figure 8b–e). Note that Figure 8b is in a log scale to show the saturation effect of 121.6 nm intensity.

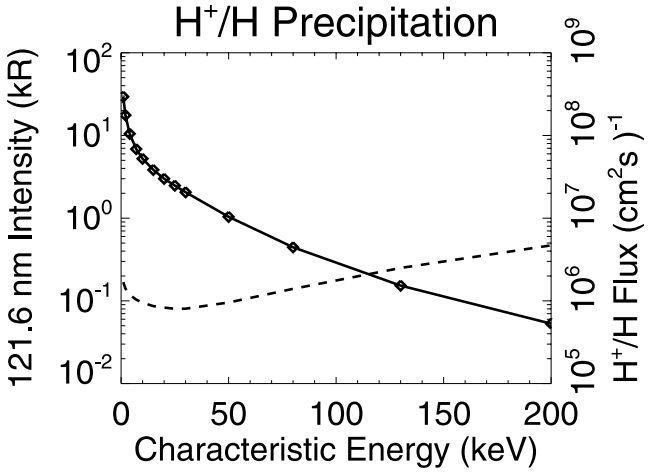

Figure 9. A plot of B3C simulated 121.6 nm intensity (solid line) viewed from a satellite versus proton or hydrogen characteristic energy (1–200 keV) with a fixed energy flux at 1.0 ergs/s/cm^2. The dashed line is for the total ENA (H^+ or H) number flux that is needed to generate the 121.6 nm emissions with an intensity of 500 Rayleigh.

produce the observed NPA intensities. A fundamental limitation is the paucity of cross section information for the energy degradation and emission processes.

[30] **Acknowledgments.** Y. Zhang, L.J. Paxton, and H. Kil acknowledge the NASA TIMED/GUVI grant NA6511412. P.C. Brandt acknowledges NSF grant ATM-0302529.

[31] Arthur Richmond thanks Marina Galand and another reviewer for their assistance in evaluating this paper.

References

Abreu, V. J., R. W. Eastes, J. H. Yee, and S. C. Solomon (1986), Ultraviolet nightglow production near the magnetic equator by neutral particle precipitation, *J. Geophys. Res.*, *91*, 11,365.

Barabash, S. (1995), Satellite observations of the plasma-neutral coupling near Mars and the Earth, Ph.D. thesis, Swed. Inst. of Space Phys., Kiruna.

Bauske, R., S. Noel, and G. W. Proelss (1997), Ionospheric storm effects in the nighttime E region caused by neutralized ring current particles, *Ann. Geophys.*, *15*, 300.

Christensen, A. B., et al. (2003), Initial observations with the Global Ultraviolet Imager (GUVI) in the NASA TIMED satellite mission, *J. Geophys. Res.*, *108*(A12), 1451, doi:10.1029/2003JA009918.

Brandt, P. C., D. G. Mitchell, Y. Ebihara, B. R. Sandel, E. C. Roelof, J. L. Burch, and R. Demajistre (2002), Global IMAGE/HENA observations of the ring current: Examples of rapid response to IMF and ring current-plasmasphere interaction, *J. Geophys. Res.*, *107*(A11), 1359, doi:10.1029/2001JA000084.

Daglis, I. A., R. M. Thorne, W. Baumjohann, and S. Orsini (1999), The terrestrial ring current: Origin, formation, and decay, *Rev. Geophys.*, *37*, 407.

Daniell, R. E., Jr. (1993), Modeling of optical signatures of electron spectra in the ionospheric heating experiments, in *Proceedings and Program for the 7th International Ionospheric Effects Symposium*, p. 6B/5/1, SRI Int., Arlington, Va.

DeMajistre, R., P. C. Brandt, T. J. Immel, J-H. Yee, A. Dalgarno, L. J. Paxton, and V. Kharchenko (2005), Storm-time enhancement of mid-latitude ultraviolet emission due to energetic neutral atom precipitation, *Geophys. Res. Lett.*, *32*, L15105, doi:10.1029/2005GL023059.

Fu, S. Y., B. Wilken, Q. G. Zong, and Z. Y. Pu (2001), Ion composition ariations in the inner magnetosphere: Individual and collective storm effects in 1991, *J. Geophys. Res.*, *106*, 29,683.

Ishimoto, M., C.-I. Meng, G. R. Romick, and R. E. Huffman (1989), Doppler shift of auroral Lyman α observed from a satellite, *Geophys. Res. Lett.*, *16*, 143.

Knudsen, W. C. (1970), Tropical ultraviolet nightglow from oxygen ion-ion neutralization, *J. Geophys. Res.*, *75*, 3862.

MacMahon, R. M., and W. D. Gonzalez (1997), Energetics during the main phase of geomagnetic superstorms, *J. Geophys. Res.*, *102*, 14,199.

Meier, R. R., and C. S. Weller (1975), Observations of equatorial EUV bands: Evidence for low-altitude precipitation of ring current helium, *J. Geophys. Res.*, *80*, 2813.

Mitchell, D. G., et al. (1998), The Imaging Neutral Camera for the Cassini Mission to Saturn and Titan, in *Measurement Techniques in Space Plasmas: Fluids*, *Geophys. Monogr. Ser.*, vol. 103, edited by R. F. Pfaff et al., p. 281, AGU, Washington, D. C.

Mitchell, D. G., et al. (2000), High-energy neutral atom (HENA) imager for the IMAGE mission, *Space Sci. Rev.*, *91*, 67.

Mitchell, D. G., K. C. Hsieh, C. C. Curtis, D. C. Hamilton, H. D. Voss, E. C. Roelof, and P. C:son-Brandt (2001), Imaging two geomagnetic storms in energetic neutral atoms, *Geophys. Res. Lett.*, *28*, 1151.

Noel, S., and G. W. Proelss (1993), Heating and radiation production by neutralized ring current particles, *J. Geophys. Res.*, *98*, 17,317.

Paresce, F. (1979), EUV observations of the equatorial aurora, *J. Geophys. Res.*, *84*, 4409.

Paxton, L. J., and C.-I. Meng (1999), Auroral imaging and space-based optical remote sensing, *Johns Hopkins APL Tech. Dig.*, *20*, 556.

Paxton, L. J., et al. (1999), Global ultraviolet imager (GUVI): Measuring composition and energy inputs for the NASA Thermosphere Ionosphere Mesosphere Energetics and Dynamics (TIMED) mission, *Proc. SPIE Int. Soc. Opt. Eng.*, *3756*, 256–276.

Paxton, L. J., et al. (2004), GUVI: A hyperspectral imager for geospace, *Proc. SPIE Int. Soc. Opt. Eng.*, *5660*, 227, doi:10.1117/12.579171.

Rassoul, H. K., R. P. Rohrbaugh, B. A. Tinsley, and D. W. Slater (1993), Spectrometric and photometric observations of low-latitude aurorae, *J. Geophys. Res.*, *98*, 7695.

Roelof, E. C. (1987), Energetic neutral atom image of a storm-time ring current, *Geophys. Res. Lett.*, *14*, 652.

Roelof, E. C., and A. J. Skinner (2000), Extraction of ion distribution from magnetospheric ENA and EUV images, *Space Sci. Rev.*, *91*, 436.

Roelof, E. C., D. G. Mitchell, and D. J. Williams (1985), Energetic neutral atoms (E ∼ 50 keV) from the ring current: IMP 7/8 and ISEE I, *J. Geophys. Res.*, *90*, 10,991.

Rohrbaugh, R. P., B. A. Tinsley, H. Rassoul, Y. Sahai, N. R. Teixeira, R. G. Tull, D. R. Doss, A. L. Cochran, W. D. Cochran, and E. S. Barker (1983), Observations of optical emissions from precipitation of energetic neutral atoms and ions from the ring current, *J. Geophys. Res.*, *88*, 6317.

Stephan, A. W., S. Chakrabarti, K. F. Dymond, S. A. Budzien, S. E. Thonnard, and R. P. McCoy (2001), Far ultraviolet equatorial aurora during geomagnetic storms as observed by the Low-Resolution Airglow and Aurora Spectrograph, *J. Geophys. Res.*, *106*, 30,323.

Stephan, A. W., et al. (2004), Oxygen aurora during the recovery phase of a major geomagnetic storm, *J. Geophys. Res.*, *109*, A09208, doi:10.1029/2004JA010557.

Tinsley, B. A. (1979), Energetic neutral atom precipitation during magnetic storms: Optical emission, ionization, and energy deposition at low and middle latitudes, *J. Geophys. Res.*, *84*, 1855.

Tinsley, B. A., and R. G. Burnside (1981), Precipitation of energetic neutral hydrogen atoms at Arecibo during a magnetic storm, *Geophys. Res. Lett.*, *8*, 87.

Torr, M. R., and D. G. Torr (1979), Energetic oxygen: A direct coupling between mechanism between the magnetosphere and thermosphere, *Geophys. Res. Lett.*, *6*, 700.

Torr, M. R., and D. G. Torr (1984), Energetic oxygen in the mid-latitude aurora, *J. Geophys. Res.*, *89*, 5547.

Zhang, Y., L. J. Paxton, D. Morrison, B. Wolven, H. Kil, and S. Wing (2005), Nightside detached auroras due to precipitating protons/ions during intense magnetic storms, *J. Geophys. Res.*, *110*, A02206, doi:10.1029/2004JA010498.

P. C. Brandt, H. Kil, L. J. Paxton, and Y. Zhang, Johns Hopkins University Applied Physics Laboratory, 11100 Johns Hopkins Road, Laurel, MD 20723, USA. (yongliang.zhang@jhuapl.edu)

J. U. Kozyra, Space Physics Research Laboratory, University of Michigan, Ann Arbor, MI 48109, USA.